aerospace

MDPI

Article

Development of RP-3 Surrogate Fuels via Multi-Objective Genetic Algorithm for Regenerative Cooling CFD with Supercritical Property Fidelity

Sangho Ko [1], Yuchang Gil [2] and Sungwoo Park [3,*]

[1] Department of Aerospace and Mechanical Engineering, Korea Aerospace University, Goyang 10540, Republic of Korea; ksh7970@kau.kr
[2] Department of Smart Air Mobility, Korea Aerospace University, Goyang 10540, Republic of Korea; yuchang.gil@kau.kr
[3] School of Aerospace and Mechanical Engineering, Korea Aerospace University, Goyang 10540, Republic of Korea
* Correspondence: sungwoo.park@kau.ac.kr

Abstract

Supercritical heat transfer in regenerative cooling channels is strongly influenced by thermophysical property variations near the pseudo-critical temperature, yet their direct implications for cooling performance have not been fully addressed. This study investigates how incorporating supercritical property considerations into surrogate fuel formulation affects heat transfer behavior in a regenerative cooling channel. RP-3 surrogate fuels were constructed using a genetic algorithm by matching both temperature-independent properties and temperature-dependent properties under supercritical conditions. Unlike previous approaches employing distillation curves as a secondary objective, the present formulation adopted supercritical density distribution and pseudo-critical temperature (T_{pc}) as optimization targets. The formulated surrogate fuels were evaluated in a regenerative cooling channel model surrounding a combustor, and their flow and heat transfer characteristics were compared with those of literature-based surrogate fuels. The results show that differences in T_{pc} and density variation trends significantly influence buoyancy-induced asymmetric flow structures and the onset of heat transfer deterioration. Surrogate fuels with lower T_{pc} exhibit earlier density reduction and earlier development of asymmetric flow, whereas fuels with higher T_{pc} demonstrate relatively mitigated wall temperature rise. The results of the present study suggest that surrogate fuel formulation based on supercritical thermophysical properties can have a significant influence on the predicted heat transfer behavior in regenerative cooling channels under the operating conditions considered.

Keywords: regenerative cooling channel; surrogate fuel; genetic algorithm; supercritical heat transfer; pseudo-critical temperature; heat transfer deterioration

Check for updates

Academic Editor: Kyun Ho Lee

Received: 27 February 2026
Revised: 20 March 2026
Accepted: 24 March 2026
Published: 25 March 2026

Copyright: © 2026 by the authors. Licensee MDPI, Basel, Switzerland. This article is an open access article distributed under the terms and conditions of the Creative Commons Attribution (CC BY) license.

1. Introduction

Scramjet engines are exposed to severe thermal loads caused by aerodynamic heating during flight as well as combustion and high-speed flow within the combustor. Such extreme thermal environments directly affect not only engine performance but also structural integrity and operational safety, making effective thermal management technologies essential [1,2]. One widely adopted approach to address these thermal challenges is the use of regenerative cooling channels [3]. In this cooling method, jet fuel is employed as

a coolant prior to combustion, absorbing heat generated inside the engine and thereby mitigating thermal loads. Under hypersonic flight conditions, the fuel flowing through regenerative cooling channels is subjected to high temperature and high pressure, which may cause it to exceed its critical point and enter a supercritical state. Supercritical fuels exhibit flow and heat transfer characteristics that differ significantly from those of conventional liquid fuels, and these changes can strongly influence cooling performance and fuel delivery behavior [4,5]. Therefore, a thorough understanding of supercritical fuel behavior within regenerative cooling channels is essential for the reliable and stable operation of scramjet engines.

Jet fuel is typically supplied at pressures above its critical pressure to ensure stable engine operation. As it is heated within the regenerative cooling channel, its thermophysical properties, including density, viscosity, thermal conductivity, and specific heat, vary significantly with temperature [6]. In particular, near the pseudo-critical temperature (T_{pc}), which is defined by the operating pressure, property gradients become highly amplified, leading to pronounced changes in flow behavior and heat transfer characteristics. The sharp decrease in density observed near T_{pc} induces buoyancy effects within the channel, which can result in asymmetric flow features such as the formation of secondary flows and dead zones [7]. These buoyancy-driven flow structure changes can contribute to localized heat transfer deterioration (HTD) and elevated wall temperatures, thereby increasing uncertainty in regenerative cooling predictions unless near T_{pc} property variations are represented with sufficient fidelity [8]. Consequently, accurate representation of temperature-dependent fuel properties is essential for reliable CFD prediction of regenerative cooling behavior under supercritical conditions.

In this context, numerous studies have investigated supercritical heat transfer using single-component surrogate fuels such as *n*-decane and *n*-dodecane as substitutes for real jet fuels [9–11]. However, RP-3 fuel, one of the practical jet fuels, is a complex mixture composed of a large number of hydrocarbon species [12], and its physicochemical characteristics cannot be fully represented by a single-component fuel. As a result, numerical simulations commonly adopt surrogate fuels composed of a limited number of representative hydrocarbons to simplify chemical composition while effectively reproducing the key properties of real fuels. This approach not only reduces computational cost but also enhances the reliability of simulation results [13].

Previous studies on surrogate fuel formulation for jet fuels have primarily considered temperature-independent properties such as molecular weight, cetane number, lower heating value (LHV), threshold sooting index (TSI), and H/C ratio, together with temperature-dependent properties such as density and viscosity [14–17]. However, in supercritical heat transfer analyses within regenerative cooling channels, the continuity, momentum, and energy equations are all strongly coupled through temperature-dependent thermophysical properties. If these property variations are not properly accounted for, the characteristic supercritical behavior cannot be accurately predicted. This includes the location of the pseudo-critical transition, buoyancy-induced asymmetric flow, and localized heat transfer deterioration [18]. To realistically simulate supercritical heat transfer behavior in regenerative cooling channels, precise evaluation and application of temperature-dependent fuel properties are required.

Accordingly, in this study, RP-3 surrogate fuels are constructed by comparing and evaluating both temperature-independent properties and temperature-dependent properties under supercritical conditions against experimental data of real RP-3 fuel [19–21]. The heat transfer behavior in a regenerative cooling channel is then investigated using the formulated surrogates. For surrogate fuel formulation, the genetic algorithm framework is adopted from Son et al. [22].

Although the prior study employed the distillation curve as the second-stage objective, its relevance to supercritical flow characteristics in regenerative cooling channels may be limited, as the distillation curve primarily reflects subcritical volatility behavior. In regenerative cooling channels, however, the fuel typically flows at pressures above its critical pressure. Under such conditions, heat transfer characteristics are governed by strong temperature-dependent property variations near the pseudo-critical region. Therefore, accurately capturing the supercritical density variation and the pseudo-critical temperature (T_{pc}) is essential for predicting the flow and heat transfer behavior.

For this reason, the present study adopts the temperature-dependent density variation under supercritical conditions together with the pseudo-critical temperature (T_{pc}) as the second objective criterion. In this study, the term 'supercritical property fidelity' refers to the capability of a surrogate fuel to reproduce the thermophysical property variations in real RP-3 fuel in the supercritical regime, particularly the density variation and the location of the pseudo-critical temperature. While temperature-independent properties ensure the overall chemical similarity of the surrogate fuel, temperature-dependent properties determine the thermophysical behavior governing supercritical heat transfer.

The resulting surrogate fuels are compared with literature-reported RP-3 surrogate formulations from Son et al. [22] and Dagaut [23], which were selected as representative literature-based surrogates constructed using different surrogate design strategies. Through this comparison, the present study examines how differences in surrogate thermophysical properties influence the predicted flow and heat transfer characteristics in the regenerative cooling channel model shown in Figure 1.

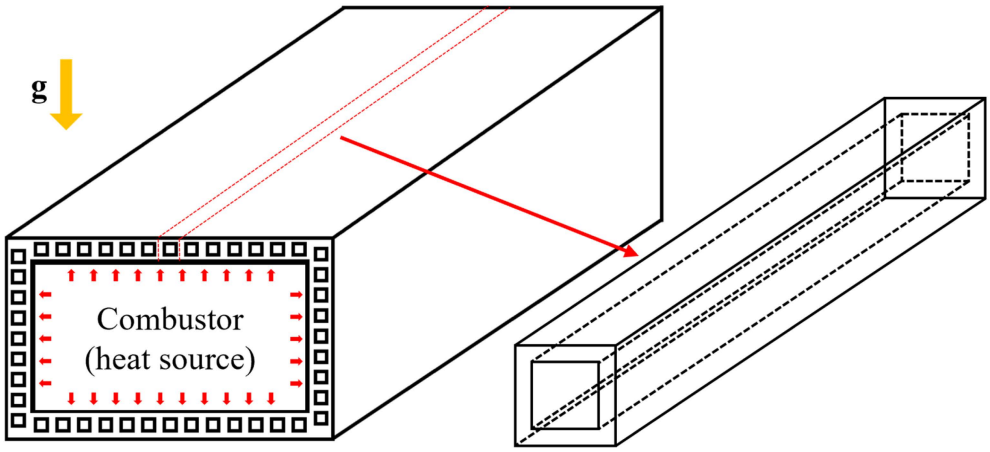


Figure 1. Schematic of regenerative cooling channel.

While these surrogate formulations successfully reproduce several conventional target properties of RP-3, their formulation criteria primarily focus on temperature-independent properties or subcritical property matching. By incorporating supercritical density behavior together with T_{pc} as optimization targets, the proposed strategy better preserves the rapid property variations near the pseudo-critical region. These variations play an important role in buoyancy-driven flow asymmetry and heat transfer deterioration under supercritical conditions. Consequently, this approach enhances the supercritical property fidelity of the formulated surrogate fuels and improves the reliability of regenerative cooling predictions.

2. Formulation of Surrogate Fuel

2.1. Genetic Algorithm Mechanism

In this study, a genetic algorithm (GA), one of the optimization techniques, was employed to formulate surrogate fuels for RP-3 fuel, and the overall methodology was

adopted from a previous study [22]. GA is a population-based stochastic optimization method inspired by the principles of natural selection and genetics, and it is particularly effective for problems involving discrete design variables and highly nonlinear objective functions. In the present work, each individual in the population is defined as a surrogate fuel candidate, represented by a combination of selected chemical species and their corresponding mole fractions.

Unlike conventional approaches that optimize only the mole fractions within a predefined set of chemical species, the referenced study defined in advance a chemical species palette representing four fuel classes—*n*-alkanes, *iso*-alkanes, *cyclo*-alkanes, and aromatics, as detailed in Table A1. Each class was selected to represent the major hydrocarbon families constituting real jet fuels. During the initial population generation stage, one chemical species is randomly selected from each class to construct a four-component surrogate fuel. During the optimization process, each individual is assigned a distinct set of mole fractions, enabling simultaneous optimization of both the constituent species and their mole fractions.

A schematic of the overall optimization procedure is shown in Figure 2. It summarizes the two-stage GA framework of Son et al. [22], where Method A denotes the first-stage GA evolution based on temperature-independent targets, and Method B represents the second-stage screening using temperature-dependent criteria (distillation curve in [22], replaced here by the supercritical density profile and T_{pc}). The GA process begins with the generation of an initial population, after which the fitness of each individual is evaluated using objective functions defined based on the agreement between surrogate fuel properties and those of real RP-3 fuel. Based on the fitness evaluation, a selection operator is applied to preferentially pass superior individuals to the next generation, followed by crossover and mutation operations to generate new individuals. The crossover operation exchanges mole-fraction information between parent individuals to explore new compositional combinations, while the mutation operation introduces random variations into the composition to prevent premature convergence and maintain population diversity.

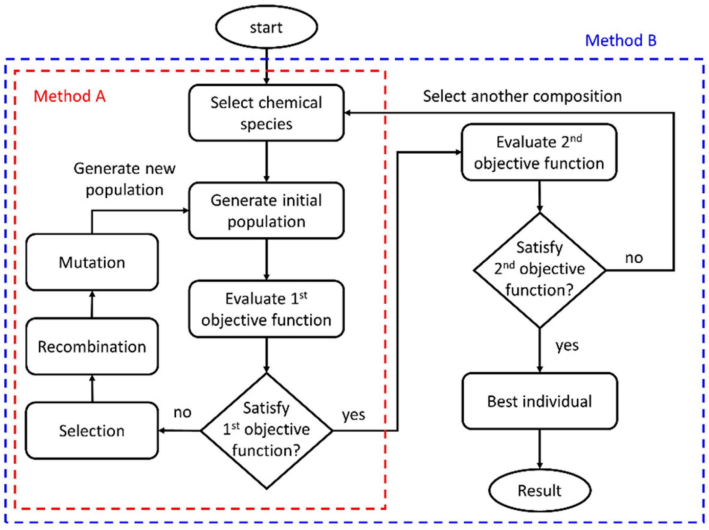


Figure 2. Two-stage GA flowchart (Method B: second objective screening) adapted from [22].

This sequence of fitness evaluation, selection, crossover, and mutation is repeated until convergence criterion is satisfied or a predefined maximum number of generations is reached. Through this evolutionary process, the GA progressively identifies surrogate fuel candidates that exhibit improved agreement with the thermophysical properties of the target fuel. Detailed GA parameters are summarized in Table A2.

2.2. Evaluation of Surrogate Fuel Fitness

The most distinctive feature of the surrogate fuel formulation strategy proposed in the previous study [22] is the adoption of a two-stage objective function structure: the first objective function targets temperature-independent properties (MW, DCN, LHV, TSI, H/C ratio, and density at 298.15 K), whereas the second employs a temperature-dependent criterion, namely the distillation curve. This two-stage surrogate formulation approach has been successfully applied to various jet fuels, including POSF-10325, JP-8, and RP-3, thereby demonstrating its scalability and applicability to a wide range of aviation fuels.

In the present study, the two-stage objective function framework proposed by Son et al. [22] is retained, while the evaluation metrics are redefined to more effectively reflect supercritical thermophysical property behavior relevant to regenerative cooling. The first-stage metrics are MW, DCN, LHV, TSI, and H/C ratio. To capture thermophysical property behavior under subcritical–supercritical conditions, the supercritical temperature-dependent density profile over the temperature range of 300–800 K at an operating pressure of 3 MPa is employed as the second-stage criterion, in place of the distillation curve used in [22]. Since the regenerative cooling simulations in the present study were conducted at an operating pressure of 3 MPa, the density profile used in the second-stage objective was evaluated at the same pressure to ensure accurate reproduction of thermophysical property variations under the relevant supercritical condition. Density was selected as a representative temperature-dependent property because buoyancy effects play an important role in supercritical heat transfer within regenerative cooling channels when gravity is considered. Since buoyancy forces are directly proportional to density differences, accurately reproducing the density variation in the coolant is essential for capturing buoyancy-driven flow asymmetry and the associated heat transfer characteristics. In addition, to quantitatively represent the region where thermophysical properties exhibit rapid variation, the pseudo-critical temperature (T_{pc}), defined as the temperature at which the constant-pressure specific heat reaches its maximum, is considered as an additional evaluation metric. Here, the second-stage metrics (density MAE and T_{pc} error) are imposed as feasibility constraints, and the final surrogate is selected among feasible candidates based on the first-stage objective. A comparison of the objective function evaluation metrics adopted in the previous study and the present study is summarized in Table 1.

Table 1. Evaluation metrics for each objective function.

	First Function	**Second Function**
Son et al. [22]	MW, DCN, LHV, TSI, H/C, Density at 298.15 K	Temperature at distilled volumes of 10%, 30%, 45%, 60%, 80%
Present study	MW, DCN, LHV, TSI, H/C	Density MAE, T_{pc} at 3 MPa

2.2.1. Calculation of Temperature-Independent Thermophysical Properties

In the genetic algorithm optimization process, each surrogate fuel candidate has a distinct chemical composition and mole fraction distribution. To evaluate the first-stage temperature-independent property targets, the mixture properties were calculated from the component properties using the mixing rules and weighting factors presented in Table 2. The weighting factors, which reflect the relative importance of each target property, were adopted from the previous study [22].

Table 2. Methods for estimating the mixture properties and weighting factors (w_t).

Target Property	Estimation Method	Weighting Factor (w_t)	Target Value [24,25]
MW [kg/kmol]	$MW_{mix} = \sum x_i MW_i$	10	145.5
DCN	$DCN_{mix} = \sum v_i DCN_i$	10	43.3
LHV [MJ/kg]	$LHV_{mix} = \sum m_i LHV_i$	1	42.4
TSI	$TSI_{mix} = \sum x_i TSI_i$	10	24.0
H/C ratio	$H/C\ ratio_{mix} = \frac{\sum x_i H_n}{\sum x_i C_n}$	1	1.96

x_i = mole fraction, m_i = mass fraction, v_i = liquid volume fraction.

In the corresponding formulations, x_i, v_i, and m_i denote the mole fraction, liquid volume fraction, and mass fraction of component i, respectively, while H_n and C_n represent the numbers of hydrogen and carbon atoms in component i. Using these relations, key fuel properties including molecular weight, derived cetane number (DCN), lower heating value (LHV), threshold sooting index (TSI), and H/C ratio were evaluated. Based on these calculated properties, the first objective function was formulated with a screening criterion such that only candidates exhibiting errors within ±3% of the target values for all properties were retained.

2.2.2. Calculation of Temperature-Dependent Thermophysical Properties

During the genetic algorithm optimization process, each surrogate fuel candidate has a distinct chemical composition and mole fraction distribution, resulting in different thermodynamic properties. To evaluate these properties efficiently within the GA loop, equation-based property models that are directly implementable in numerical codes are required. The Redlich–Kwong Peng–Robinson (RK-PR) equation of state [26,27] is employed to calculate density and constant-pressure specific heat under supercritical conditions. The governing equations and formulations used for the density and specific heat calculations are presented below.

$$P = \frac{\rho R_u T}{M - b\rho} - \frac{a\alpha(T)\rho^2}{(M + \delta_1 b\rho)(M + \delta_2 b\rho)} \tag{1}$$

$$c_p = c_v + \frac{T}{\rho^2}\left[\left(\frac{\partial P}{\partial T}\right)_\rho^2 \left(\frac{\partial P}{\partial \rho}\right)_{T,Y}^{-1}\right] \tag{2}$$

The RK-PR equation of state provides thermodynamic state variables and related properties for multi-component mixtures through appropriate mixing and combining rules, allowing the mixture to be represented as a pseudo-pure substance under both subcritical and supercritical conditions. Among the available mixing rules, the present study adopts the formulation summarized in the following equations.

$$\frac{\partial a_{ij}\alpha_{ij}}{\partial T} = \sqrt{a_i a_j}\frac{\partial \sqrt{\alpha_i \alpha_j}}{\partial T} = \sqrt{a_i a_j}\left(\frac{1}{2}\sqrt{\frac{\alpha_i}{\alpha_j}}\frac{\partial \alpha_j}{\partial T} + \frac{1}{2}\sqrt{\frac{\alpha_j}{\alpha_i}}\frac{\partial \alpha_i}{\partial T}\right) \tag{3}$$

$$\frac{\partial^2 a_{ij}\alpha_{ij}}{\partial T^2} = \sqrt{a_i a_j}\frac{\partial^2 \sqrt{\alpha_i \alpha_j}}{\partial T^2} = \sqrt{a_i a_j}\left[\frac{1}{2\sqrt{\alpha_i \alpha_j}}\frac{\partial \alpha_i}{\partial T}\frac{\partial \alpha_j}{\partial T} - \frac{1}{4}\sqrt{\frac{\alpha_i}{{\alpha_j}^3}}\left(\frac{\partial \alpha_j}{\partial T}\right)^2 - \frac{1}{4}\sqrt{\frac{\alpha_j}{{\alpha_i}^3}}\left(\frac{\partial \alpha_i}{\partial T}\right)^2 + \frac{1}{2}\sqrt{\frac{\alpha_i}{\alpha_j}}\frac{\partial^2 \alpha_j}{\partial T^2} + \frac{1}{2}\sqrt{\frac{\alpha_j}{\alpha_i}}\frac{\partial^2 \alpha_i}{\partial T^2}\right] \tag{4}$$

The detailed formulations of the RK-PR parameters and the associated mixing rules are provided in Refs. [26,27]. The RK-PR equation of state has been reported to provide reasonable accuracy for hydrocarbon mixtures over a wide range of conditions, making it suitable for predicting the thermophysical properties required for supercritical heat-transfer analyses.

For density, the mean absolute error (MAE) relative to the experimental RP-3 data was used as a feasibility criterion in the second-stage screening to uniformly quantify errors over 300–800 K at 3 MPa. In addition, since T_{pc} is defined as the temperature at which the constant-pressure specific heat reaches its maximum under a given pressure [28], the temperature corresponding to the maximum specific heat calculated by RK-PR was taken as the surrogate T_{pc}, and its deviation from the experimental value [19] was also evaluated. The allowable thresholds for density MAE and T_{pc} error were set to 20 kg/m^3 and 10 K, respectively. These thresholds were empirically determined to ensure stable convergence and the emergence of a sufficient number of feasible surrogate candidates. In parallel, they were designed to impose an error tolerance for density and T_{pc} comparable to that adopted in the first-stage objective function, based on deviations relative to their respective target values.

2.3. Surrogate Fuels and Temperature-Independent Properties

To compare the accuracy of thermophysical property reproduction among the formulated surrogate fuels, compositional and property comparisons were conducted with surrogate fuels proposed in previous studies as well as a literature-based surrogate fuel. The surrogate fuels proposed in the referenced study [22], which follows the same formulation methodology, are denoted as 'Son-1' and 'Son-2'. By comparison, the surrogate fuel newly formulated in the present study with consideration of supercritical thermophysical properties is denoted as 'Present'. In addition, a literature-based surrogate derived from experimental thermophysical properties of RP-3 fuel [23] is denoted as 'Dagaut'.

The compositions of the surrogate fuels are summarized in Table 3, showing distinct chemical compositions among the surrogates. The Dagaut surrogate was formulated without class-based constraints and thus does not include *iso*-alkanes. In contrast, Son-1 and Son-2 were formulated under an imposed target molecular weight (MW) of 165.0 kg/kmol [24], yielding higher MW than the other surrogates; this constraint also explains their relatively large MW deviation in Table 4. The mixture properties reported in Tables 3 and 4 were calculated from species properties adopted from the referenced study [22] using the mixing rules described in Table 2.

Table 3. Chemical compositions (mole fractions) and temperature-independent properties of the surrogate fuels.

	Present-1	**Present-2**	**Son-1 [22]**	**Son-2 [22]**	**Dagaut [23]**
n-decane					0.191
n-dodecane	0.386	0.351		0.355	0.365
n-tetradecane			0.270		
iso-dodecane		0.142	0.359		
iso-cetane	0.087			0.205	
decalin			0.181	0.249	
ethylcyclohexane		0.244			
methylcyclohexane	0.273				0.145
tetralin			0.188		
1,2,4-trimethylbenzene				0.189	
n-butylbenzene	0.253	0.263			0.299
MW [kg/kmol]	146.4	146.6	164.0	164.6	143.7
DCN	43.3	43.2	43.3	43.4	51.3
LHV [MJ/kg]	43.6	43.6	43.4	43.3	43.6
TSI	24.1	24.2	24.0	24.1	24.4
H/C	1.945	1.944	1.950	1.950	1.934

Table 4. Errors in temperature-independent properties relative to RP-3.

	MW [kg/kmol]		DCN		LHV [MJ/kg]		TSI		H/C	
RP-3 [24,25]	**145.5**		**43.3**		**42.4**		**24.0**		**1.960**	
	Value	**% Error**	**Value**	**% Error**	**Value**	**% Error**	**Value**	**% Error**	**Value**	**% Error**
Present-1	146.4	0.61	43.3	0.07	43.6	2.78	24.1	0.41	1.945	0.77
Present-2	146.6	0.79	43.2	0.14	43.6	2.76	24.2	0.76	1.944	0.82
Son-1 [22]	164.0	12.7	43.3	0	43.4	2.36	24.0	0	1.950	0.51
Son-2 [22]	164.6	13.1	43.4	0.23	43.3	2.12	24.1	0.42	1.950	0.51
Dagaut [23]	143.7	1.22	51.3	18.51	43.6	2.79	24.4	6.02	1.934	1.33

As summarized in Table 4, the present surrogates exhibit errors within 3% for all temperature-independent properties. By comparison, relatively large deviations are observed in the derived cetane number (DCN) and threshold sooting index (TSI) for the Dagaut surrogate. These discrepancies may be attributed to its distinct chemical composition, particularly the relatively high contribution of normal-alkane species, which tends to increase DCN and alter sooting-related indices.

2.4. Comparison of Thermophysical Properties

Under the high-temperature and high-pressure conditions relevant to regenerative cooling, thermophysical properties of the fuel can vary rapidly with temperature. Among these properties, density, viscosity, thermal conductivity, and constant-pressure specific heat critically influence the flow behavior and heat transfer characteristics in the channel. Prior to the heat-transfer analysis, we systematically compare temperature-dependent property variations arising from differences in surrogate composition.

During the surrogate fuel formulation process, the RK-PR equation of state was employed for computationally efficient, in-loop evaluation of thermophysical properties within the optimization algorithm. In contrast, in the present comparison stage, thermophysical properties were evaluated using the NIST SUPERTRAPP database [29] to ensure a consistent basis for comparison across all surrogate fuels. Previous studies [30,31] reported that RK-PR-based predictions show good agreement with SUPERTRAPP results under high-temperature and high-pressure conditions. RK-PR is adopted for iterative surrogate formulation, whereas SUPERTRAPP is used as a consistent reference for subsequent property comparison and heat-transfer analyses. A comparison of thermophysical properties predicted by the RK-PR equation of state and the NIST SUPERTRAPP database is provided in Appendix B. The resulting temperature-dependent property variations are shown in Figure 3.

All surrogate fuels exhibit trends similar to the experimental data of real RP-3 fuel [28] in the low-temperature region. As temperature increases, however, the properties change rapidly near T_{pc}, where the constant-pressure specific heat reaches its maximum. The temperature range associated with these rapid variations depends on the surrogate fuel. In particular, the T_{pc} values of the Son surrogates are approximately 30 K higher than those of Present-1, Present-2, and Dagaut, as summarized in Table 5.

Such differences in the location of rapid property variations associated with T_{pc} can lead to distinct flow behaviors in regenerative cooling channels. Specifically, density decreases sharply across the pseudo-critical region, resulting in a high-density fluid below this region and a low-density fluid above it. This density contrast can make buoyancy effects pronounced and may promote buoyancy-driven stratification under gravity [32].

Table 5. Errors in pseudo-critical temperature relative to RP-3.

RP-3 [19]	T_{pc} [K]	
	672	
	Value	% Error
Present-1	675	0.45
Present-2	677	0.74
Son-1 [22]	711	5.8
Son-2 [22]	711	5.8
Dagaut [23]	672	0

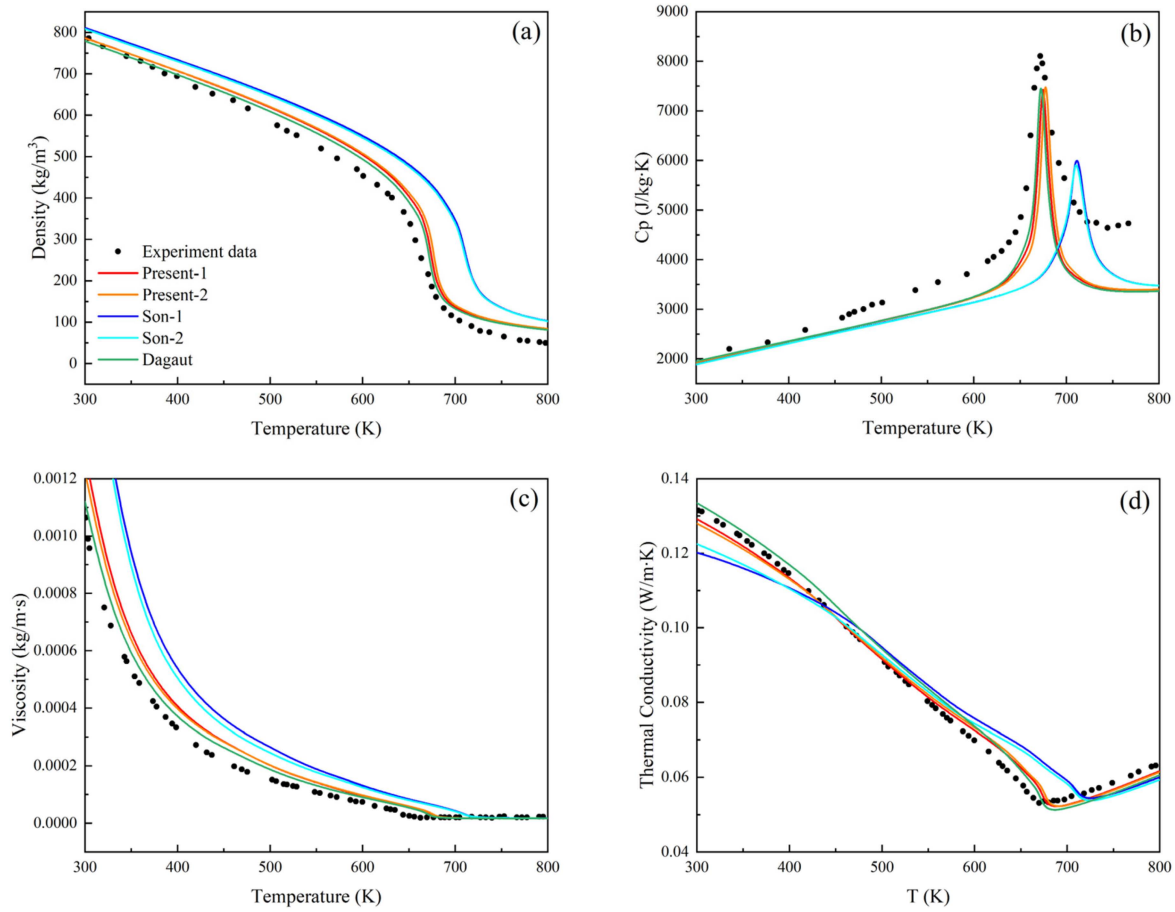


Figure 3. Thermophysical properties of surrogate fuels [22,23] and experimental data of RP-3 [28] at p = 3 MPa: (**a**) density, (**b**) specific heat capacity at constant pressure (**c**) viscosity, (**d**) thermal conductivity.

3. Supercritical Heat Transfer Analysis Using Formulated Surrogates

3.1. Computational Model and Setup

The computational domain was established with reference to [33]. Consistent with this prior work, a square cross-section cooling channel with an inner side length of 2 mm and an outer side length of 3 mm was employed, with the solid wall assumed to be made of SUS 304. The test section length was set to L_{test} = 800 mm, and a convective heat-transfer boundary condition was imposed on the outer wall of the test section to replicate a severe thermal environment representative of a hypersonic combustor. To obtain a fully developed flow before entering the test section and to minimize outlet boundary influences, additional inlet and outlet sections of L_{in} = L_{out} = 100 mm were attached upstream and downstream

of the test section, resulting in a total length of 1000 mm. A schematic representation of the computational domain is provided in Figure 4.

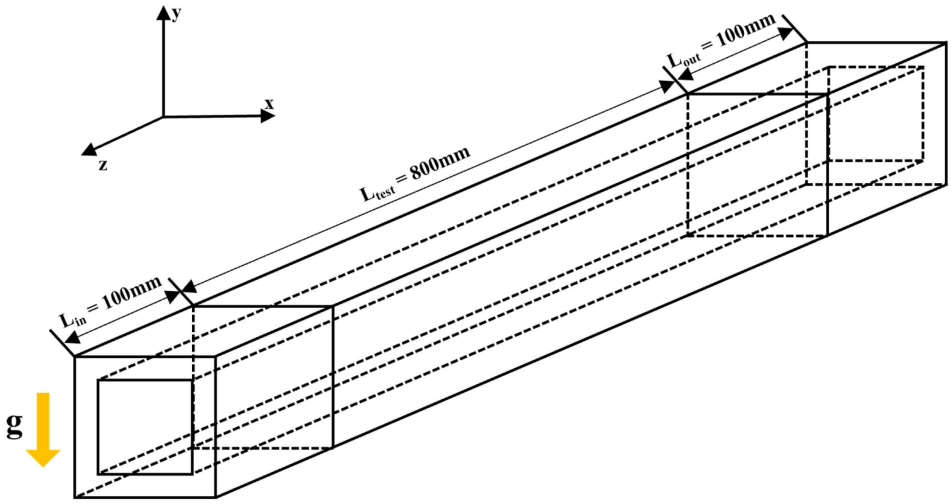


Figure 4. Schematic diagram of Computational domain.

Numerical simulations were conducted using ANSYS Fluent 2021R1. The computational mesh was generated in Ansys Meshing, as illustrated in Figure 5. The first layer height was set to 1×10^{-6} m to ensure that the non-dimensional wall distance (y+) remained below 1. The mesh was extruded along the axial direction (z-axis) with a uniform spacing of 0.5 mm, resulting in approximately 10 million cells; mesh independence was confirmed via a mesh sensitivity test, and the detailed results are summarized in Appendix C.

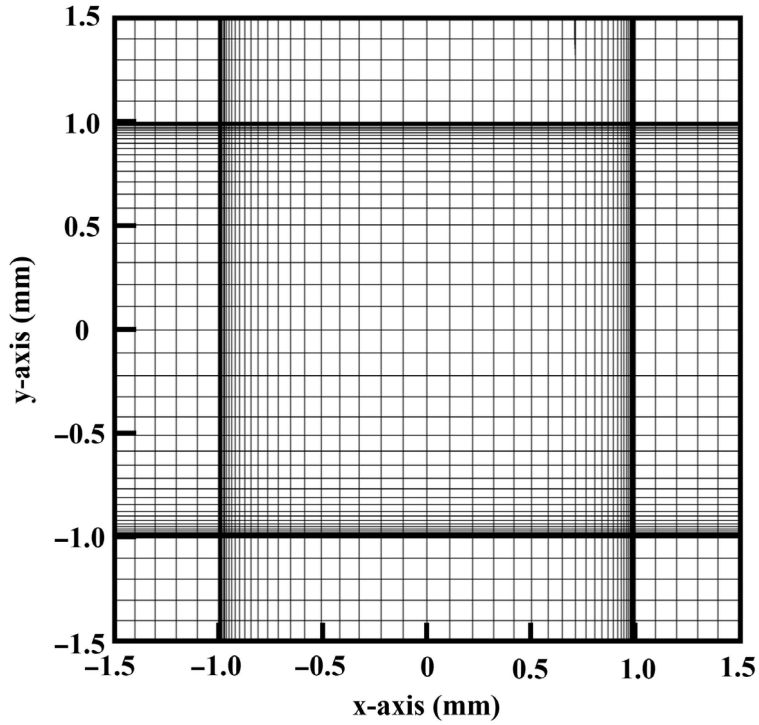


Figure 5. Mesh configuration of the regenerative cooling channel.

The thermophysical properties of each surrogate fuel at operating pressure were obtained from the NIST SUPERTRAPP database and discretized into 50 temperature points. Finer temperature intervals were applied near the pseudo-critical region to resolve rapid

property variations. The tabulated data were then implemented in ANSYS Fluent for temperature-dependent property modeling.

Simulations were performed under steady-state conditions using a pressure-based solver with the SIMPLEC algorithm, and convergence was deemed achieved when the normalized RMS residuals fell below 1×10^{-5}. Additional simulation settings were consistent with those used in the previous study [34]. The SST k–ω model was employed to capture complex flow and turbulence characteristics under supercritical conditions, providing robust predictions in both boundary layers and free shear regions. Although the inlet Reynolds number is relatively low ($Re_{in} \approx 974$), it increases rapidly as the fuel is heated, reaching $Re_{out} \approx 6.4 \times 10^4$ in the downstream heated section (region of interest). Since the primary interest of the present study lies in the strongly heated supercritical region, where large thermophysical property variations drive buoyancy-influenced turbulence and heat transfer, the use of a turbulence model is considered appropriate. Sun et al. [7] showed that the SST k–ω model can adequately reproduce HTD trends in supercritical flows with notable buoyancy and acceleration effects. The steady-state RANS equations were solved; the governing equations are given below in their general form.

Mass conservation equation:

$$\frac{\partial(\rho u_i)}{\partial x_i} = 0 \tag{5}$$

Momentum conservation equation:

$$\frac{\partial(\rho u_i)}{\partial t} + \frac{\partial(\rho u_i u_j)}{\partial x_j} = -\frac{\partial p}{\partial x_i} + \frac{\partial}{\partial x_j}\left[\mu\left(\frac{\partial u_i}{\partial x_j} + \frac{\partial u_j}{\partial x_i}\right) - \frac{2}{3}\mu\frac{\partial u_l}{\partial x_l}\delta_{ij}\right] + \rho g_i \tag{6}$$

Energy conservation equation:

$$\frac{\partial(\rho T)}{\partial t} + \frac{\partial(\rho u_i T)}{\partial x_i} = \frac{\partial}{\partial x_i}\left[\frac{\lambda}{c_p}\frac{\partial T}{\partial x_i}\right] \tag{7}$$

For turbulence closure, the transport equations for the SST k-ω model were adopted from the original formulation by Menter [35].

To perform a heat transfer analysis of the regenerative cooling channel in a scramjet engine, it is necessary to establish boundary conditions that appropriately reflect realistic operating conditions. The simulation conditions in the present study were determined based on those reported in the relevant previous study [34]. The operating pressure was set to 3 MPa, which is higher than the critical pressure of RP-3 fuel (2.33 MPa), in order to ensure supercritical pressure conditions [36]. The inlet temperature and mass flow rate were specified as 300 K and 2.5 g/s, respectively.

Heat transfer was modeled through the lower outer wall of the test section, while the remaining outer walls were treated as adiabatic. To simulate the high-temperature environment encountered in an actual combustor, a convective heat transfer boundary condition was imposed, with the hot gas temperature (T_a) and heat transfer coefficient (h_w) set to 2400 K and 1100 $W/m^2 \cdot K$, respectively [37]. The convective heat transfer relation is:

$$q_w = h_w(T_a - T_s) \tag{8}$$

where T_s denotes the wall surface temperature and q_w is convective heat flux.

Thermal pyrolysis was not considered in the present analysis. Although thermal decomposition may locally initiate under high wall-temperature conditions, it is not expected to dominate the supercritical heat transfer behavior or the overall thermophysical property trends examined in this study. The present work focuses on the influence of fuel

composition on heat transfer characteristics, and the effects of thermal pyrolysis on heat transfer behavior will be investigated in future studies.

3.2. Supercritical Thermophysical Behavior and Heat-Transfer Features

Before comparing the heat transfer characteristics among surrogate fuels, it is necessary to outline the distinct thermophysical-property variations in supercritical fluids. Under high-pressure conditions, thermophysical properties depend strongly on both temperature and pressure and can exhibit abrupt changes near the pseudo-critical region. Such property variations play a key role in governing heat transfer behavior in regenerative cooling channels.

Figure 6 illustrates the density and temperature distributions on the YZ-plane (x = 0) for the case employing the Present-1 surrogate fuel among the five surrogate fuels considered. The fluid adjacent to the directly heated lower wall experiences a preferential temperature rise, and a sharp decrease in density is observed as the fluid temperature approaches and exceeds T_{pc}. This behavior is consistent with the temperature-dependent thermophysical-property variations shown in Figure 7. Although the fluid cannot be strictly classified as liquid or gas under the present supercritical conditions, it can be described as liquid-like or vapor-like depending on its density level and the sharp property gradients near T_{pc} [38,39]. In particular, near T_{pc}, the density decreases abruptly while the constant-pressure specific heat reaches a maximum, exhibiting thermophysical variations analogous to those observed during phase change. The property differences between the liquid-like and vapor-like states play an important role in understanding heat transfer behavior in regenerative cooling channels.

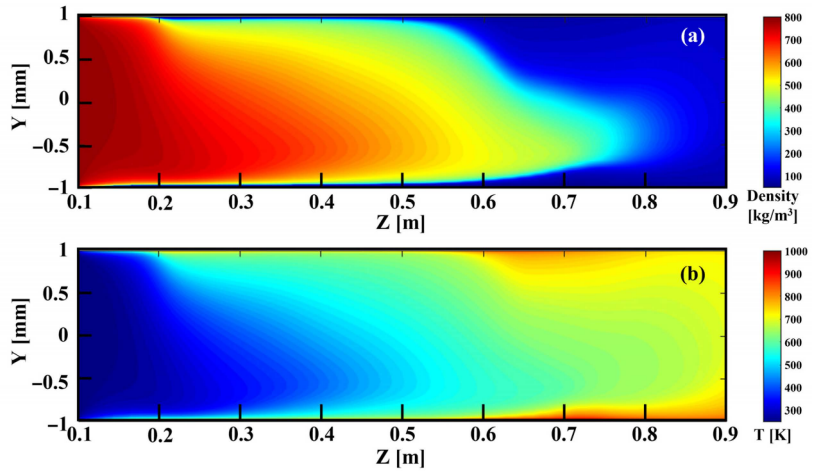


Figure 6. Contours on the YZ-plane for Present-1: (**a**) density, (**b**) temperature.

Near the channel inlet, the fluid temperature remains below T_{pc}, and the flow exhibits a liquid-like state characterized by relatively high density. As the fluid is heated along the channel and its temperature exceeds T_{pc}, the density decreases sharply and the fluid transitions to a vapor-like state. Because the vapor-like fluid has a lower density than the surrounding liquid-like fluid, the heated near-wall fluid tends to migrate toward the upper region of the flow domain under the influence of buoyancy in the presence of gravity. This buoyancy-driven motion produces a clear density stratification across the pseudo-critical region and promotes the accumulation of high-temperature fluid in the near-wall region rather than in the channel core. Owing to this buoyancy-driven redistribution, the high-temperature fluid spreads across the cross-section, even though heat is supplied only through the lower wall.

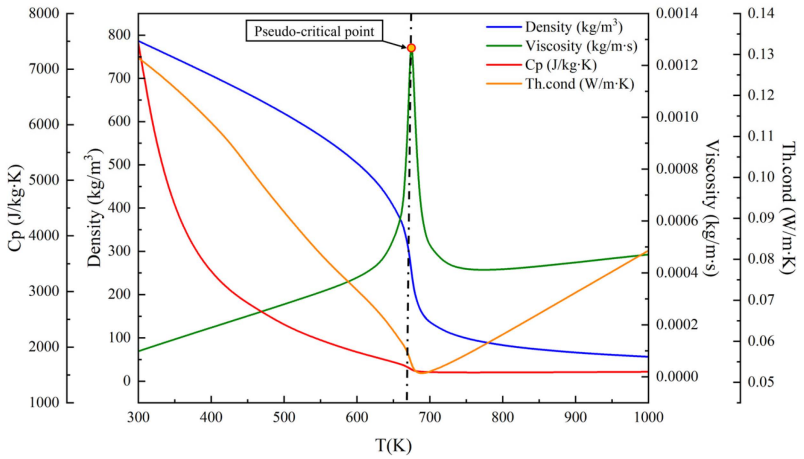


Figure 7. Thermophysical property variations in Present-1 near the pseudo-critical temperature (T_{pc}).

Further downstream, as the low-temperature core flow is progressively heated, the density difference across the cross-section gradually diminishes. Consequently, the buoyancy-driven stratification weakens, and the flow eventually approaches a nearly uniform vapor-like low-density state near the outlet.

3.3. Comparison of Heat Transfer Characteristics Among Surrogate Fuels

Based on the fundamental characteristics of supercritical heat transfer discussed in the previous section, this section analyzes the influence of surrogate fuel composition on heat transfer behavior within the regenerative cooling channel. Although all simulation cases employ identical geometric configurations, boundary conditions, and operating parameters, differences in temperature-dependent thermophysical properties, such as density, constant-pressure specific heat, viscosity, and thermal conductivity, can lead to distinct flow and heat transfer characteristics under supercritical conditions. In particular, variations in T_{pc} and the associated property trends are expected to have a notable impact on buoyancy-induced flow structures, wall temperature distributions, as well as the onset and development of heat transfer deterioration. In this section, the supercritical heat transfer characteristics of the surrogate fuels are systematically compared based on the corresponding simulation results.

As demonstrated by the temperature-dependent thermophysical property comparisons in Section 2, Son-1 and Son-2 as well as Present-1 and Present-2 exhibit nearly identical trends under the present supercritical conditions. Therefore, Son-1 and Present-1 were selected as representative cases for the heat transfer simulations, and the literature-based surrogate fuel Dagaut was additionally included, resulting in a total of three surrogate fuels considered in the comparative analysis. This case selection strategy allows for a clear evaluation of fuel-dependent heat transfer characteristics while avoiding redundant simulations.

3.3.1. Temperature and Density Distributions

Figures 8 and 9 illustrate the density and temperature contours on the YZ-plane for each surrogate fuel, respectively. In addition to the Present-1 case discussed previously, pronounced density gradients are also observed for Son-1 and Dagaut as the fluid temperature varies across T_{pc}, yielding asymmetric density/temperature fields. Furthermore, high-temperature, low-density flow develops preferentially in the region adjacent to the heated wall, and a common trend is observed in which the temperature and density distributions gradually become more uniform as the flow progresses downstream.

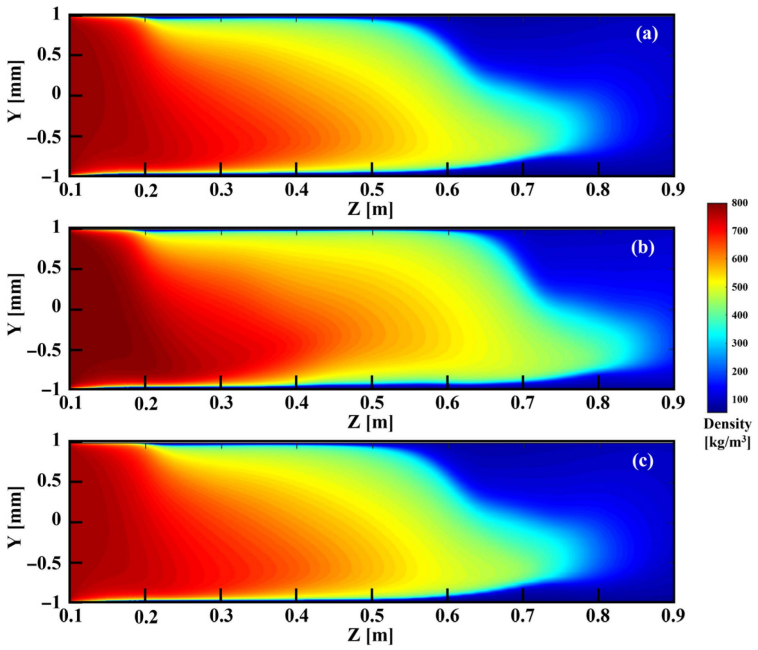


Figure 8. Density distribution on the YZ-plane for each surrogate: (**a**) Present-1, (**b**) Son-1, (**c**) Dagaut.

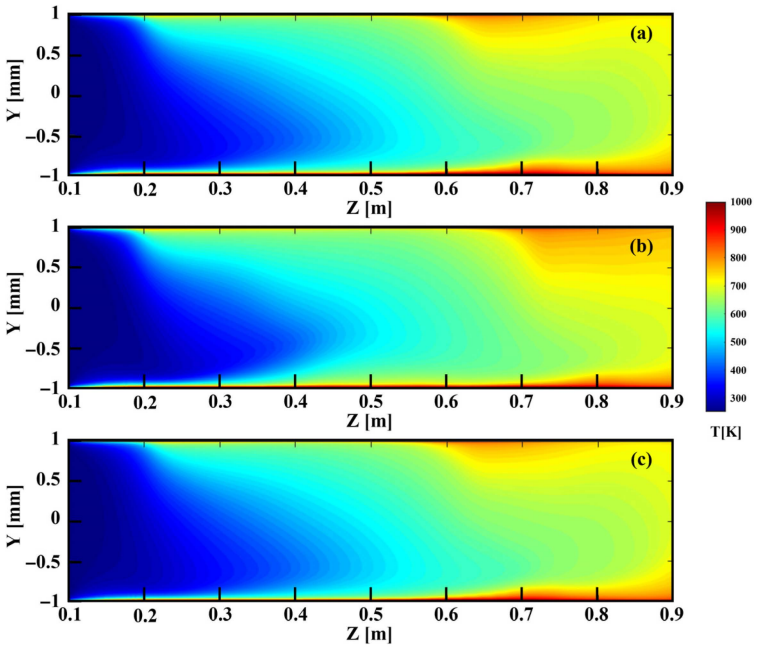


Figure 9. Temperature distribution on the YZ-plane for each surrogate: (**a**) Present-1, (**b**) Son-1, (**c**) Dagaut.

However, the locations at which pronounced density gradients form differ among the surrogate fuels, which can be attributed to differences in their T_{pc}. According to the density and constant-pressure specific heat data at the operating pressure presented earlier, T_{pc} of Son-1, Present-1, and Dagaut are 711 K, 675 K, and 672 K, respectively, with Son-1 exhibiting T_{pc} approximately 30 K higher than those of the other surrogate fuels. Such a relatively high T_{pc} delays the transition from a liquid-like state to a vapor-like state, which is clearly reflected in the density distributions on the YZ-plane.

In addition, to examine the flow structures within the channel cross section, Figure 10 presents the contours of density and streamlines. Near the channel inlet, the density of the fluid adjacent to the heated wall gradually decreases as the fluid temperature increases. In regions where high-density and low-density fluids coexist, a pronounced density gradient

develops, which can induce buoyancy-driven secondary flow. Notably, owing to its higher T_{pc}, Son-1 exhibits more persistent density stratification downstream (e.g., at z = 0.8 m), whereas Present-1 and Dagaut evolve toward a more uniform low-density state.

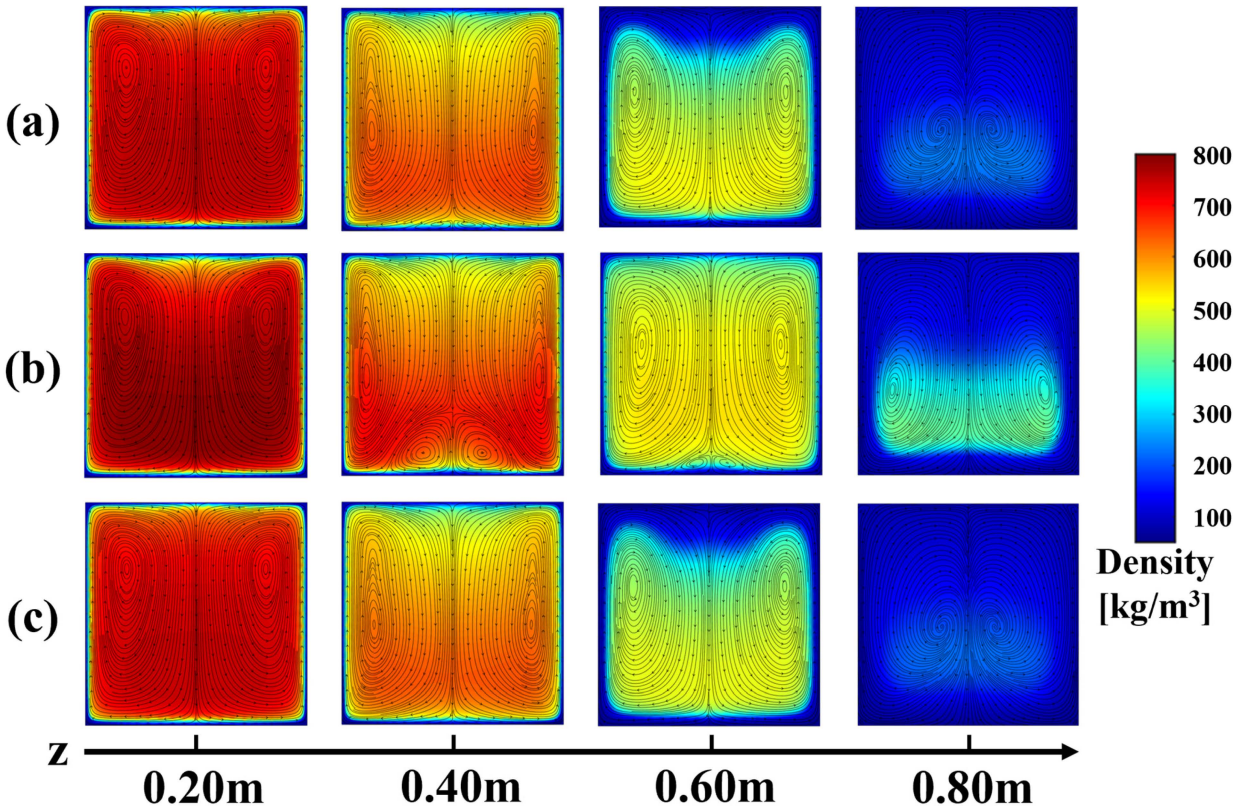


Figure 10. Density contours and streamlines on the XY-plane along the channel: (**a**) Present-1, (**b**) Son-1, (**c**) Dagaut.

As the flow proceeds downstream, the low-density fluid is distributed in the upper region of the flow domain, while the relatively high-density fluid remains near the lower part of the channel. In regions where the fluid is sufficiently heated, the temperature and density distributions become increasingly uniform, and the streamlines exhibit a relatively simple pattern. Overall, the flow behavior within the regenerative cooling channel is governed by buoyancy effects induced by density gradients and the resulting secondary flow structures.

3.3.2. Wall and Bulk Temperature Profiles

In combustion chamber cooling, the wall temperature is a key parameter governing heat transfer performance. Based on relevant literature, the wall temperature is examined along the heated wall. The wall temperature is obtained by averaging the fluid temperature in the near-wall region at each axial location in order to capture local heat transfer deterioration occurring across the channel cross-section rather than only at the heated lower wall. In this study, heat-transfer deterioration (HTD) is identified from the wall-temperature response as a region where the axial wall-temperature gradient increases markedly, which is associated with buoyancy-driven cross-sectional redistribution near the pseudo-critical region. Therefore, we use the wall-temperature profile (and the associated change in axial wall-temperature gradient) as the primary indicator to compare surrogate-fuel effects un-

der the present operating condition. The bulk temperature is defined as follows, and the resulting wall and bulk temperature distributions are presented in Figure 11.

$$T_b = \frac{\int_A \rho u c_p T dA}{\int_A \rho u c_p dA} \tag{9}$$

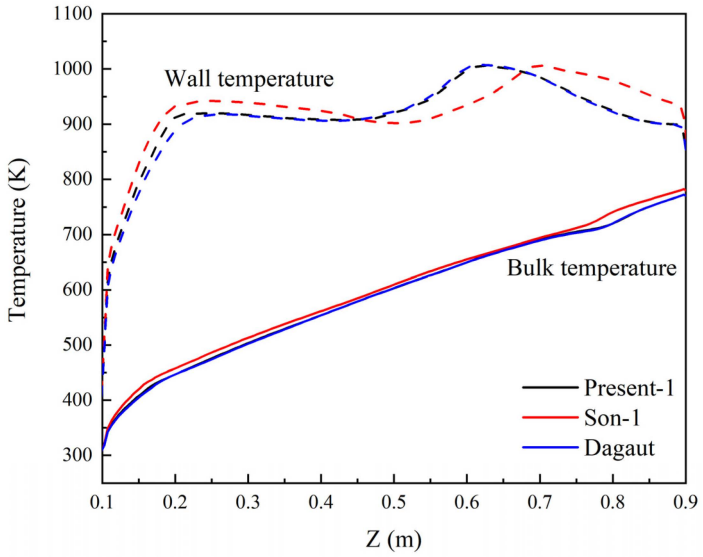


Figure 11. Wall and bulk temperature distributions for each surrogate fuel.

While the wall temperature exhibits a highly nonlinear distribution, the bulk temperature shows a relatively linear increasing trend. As mentioned earlier, buoyancy-driven migration of the low-density fluid toward the upper region of the channel produces a non-uniform flow structure across the cross-section. As a result, the heated low-density fluid accumulates in the upper region, which weakens the mixing between the near-wall fluid and the core flow. This process reduces the local convective heat transfer capability near the heated wall and promotes the development of local heat transfer deterioration, leading to a pronounced and nonlinear increase in wall temperature in regions where strong density gradients develop.

The location of the maximum wall temperature differs noticeably for Son-1 compared with the other surrogate fuels, which is attributed to differences in T_{pc}. This trend is also consistent with the density and temperature contours presented earlier. In addition, Son-1 maintains a comparatively higher wall temperature in the downstream region, which may be related to differences in temperature-dependent thermophysical properties (e.g., constant-pressure specific heat and thermal conductivity).

Considering the chemical characteristics of the fuel in regenerative cooling channels, these temperatures may be sufficiently high for thermal decomposition and coking to occur. However, since fuel pyrolysis was not considered in the present study, it is expected that incorporating endothermic pyrolysis reactions in future analyses would lead to lower wall temperatures than those obtained in the present simulations.

3.3.3. Asymmetric Flow: Streamwise Velocity Profiles

Under supercritical conditions, the flow field develops asymmetrically due to rapid variations in thermophysical properties near T_{pc} combined with buoyancy effects. To clearly analyze this flow asymmetry, the present section focuses on the streamwise velocity distributions across the channel cross section. The velocity distribution directly reflects the momentum distribution within the flow and thus provides essential information for understanding the formation of asymmetric flow structures.

Figure 12 shows the streamwise (Z-direction) velocity profiles extracted along the vertical centerline of the channel cross section at different streamwise locations. In all cases, the velocity approaches zero in the near-wall region due to the no-slip boundary condition, while higher velocities are observed toward the channel core as the flow develops. In addition, as the fluid temperature increases downstream, the fluid density decreases, leading to a gradual increase in the streamwise velocity.

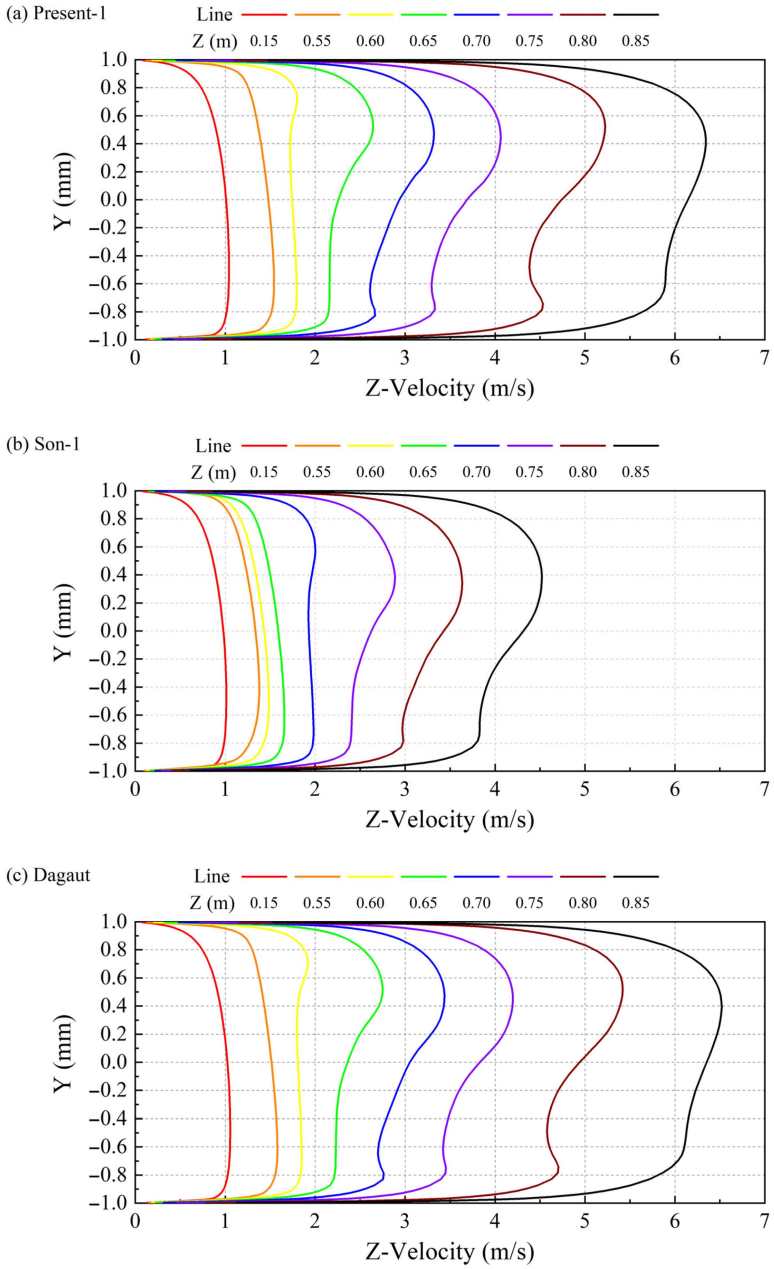


Figure 12. Streamwise velocity profiles of the centerline in the y axis direction at different position along the z axis.

In contrast, in regions where asymmetric flow structures develop within the cross section, the streamwise velocity distribution also becomes asymmetric. As shown in Figure 12, the streamwise-velocity profiles lose symmetry about the channel mid-height at certain downstream locations. At the same axial station, the upper and lower portions of the cross section exhibit noticeably different velocity levels, indicating a skewed momentum distribution. The streamwise locations at which such asymmetry appears differ among the

surrogate fuels, which is attributed to differences in T_{pc} that determine the onset of density reduction. In other words, since the locations where pronounced property variations occur near T_{pc} vary for each surrogate fuel, the streamwise velocity distributions exhibit asymmetry at different positions. This behavior originates from the density difference between the high-density core flow and the low-density near-wall flow. Under a constant mass flow rate condition, relatively higher velocities occur in low-density regions; consequently, correspondingly higher velocities are observed where low-density fluid is distributed toward the upper part of the cross section. As shown in Figure 12, this results in different velocity magnitudes along the y-direction within the cross section, clearly demonstrating the asymmetric flow structure under supercritical conditions.

4. Conclusions

In this study, supercritical heat transfer in a regenerative cooling channel was numerically investigated using GA-based RP-3 surrogate fuels. The influence of temperature-dependent thermophysical properties arising from different fuel compositions on flow and heat transfer behavior was examined. Particular attention was given to how property variations near T_{pc} under supercritical conditions are linked to buoyancy-driven flow asymmetry and heat transfer deterioration.

The comparison of thermophysical properties among the surrogate fuels showed that T_{pc}, as well as the trends in density and constant-pressure specific heat, differ depending on fuel composition. These differences extend beyond simple property variations and directly affect the flow structure and heat transfer characteristics within the regenerative cooling channel. In particular, the abrupt density reduction near T_{pc} induces a clear distinction between liquid-like and vapor-like states, which was identified as a key physical mechanism governing supercritical heat transfer behavior.

For all surrogate fuel cases, the low-density vapor-like fluid heated near the wall tended to migrate toward the upper region of the flow domain due to buoyancy effects, and secondary flows were generated as a result of the associated density gradients. Consequently, high-temperature fluid developed preferentially in the near-wall region rather than in the channel core, leading to a nonlinear wall temperature distribution and the occurrence of local heat transfer deterioration. This phenomenon was particularly pronounced in regions where strong density differences existed across T_{pc}.

Comparative analysis among the surrogate fuels revealed that the location and intensity of asymmetric flow structures and heat transfer deterioration strongly depend on T_{pc} of each fuel. For Son-1, which has a relatively higher T_{pc}, the transition from the liquid-like to the vapor-like state was delayed, and density reduction occurred further downstream, resulting in comparatively mitigated buoyancy-induced asymmetry and wall temperature rise. In contrast, for surrogate fuels with lower T_{pc}, the density reduction occurs at an earlier stage, causing the influence of buoyancy effects to appear further upstream, and consequently leading to the earlier development of asymmetric flow structures.

These results indicate that heat transfer characteristics in supercritical regenerative cooling channels are governed not only by operating conditions but also by fuel-dependent pseudo-critical behavior and thermophysical property variation trends. In this regard, surrogate fuel formulation should be regarded not merely as a means of achieving thermophysical property matching, but also as a means of preserving supercritical property fidelity, which governs the flow and heat transfer behavior in regenerative cooling channels.

It should be noted that fuel pyrolysis was not considered in the present simulations. Since the predicted wall temperatures fall within a range where thermal decomposition and coking of the fuel may occur, future studies should incorporate endothermic pyrolysis

reactions to more accurately capture the coupled effects of supercritical heat transfer and chemical reactions.

Author Contributions: Conceptualization, S.K. and S.P.; methodology, S.K. and Y.G.; software, S.K. and Y.G.; formal analysis, S.K.; investigation, S.K. and Y.G.; resources, S.K.; data curation, S.K.; writing—original draft preparation, S.K.; writing—review and editing, Y.G. and S.P.; visualization, S.K.; supervision, S.P.; project administration, S.P.; funding acquisition, S.P. All authors have read and agreed to the published version of the manuscript.

Funding: This research received no external funding.

Data Availability Statement: Data are contained within the article.

Conflicts of Interest: The authors declare no conflicts of interest.

Appendix A

The candidate chemical species for surrogate fuel formulation were selected as listed in Table A1. This palette was compiled based on literature surveys that summarize representative components widely used in jet-fuel surrogate formulations [22]. The candidate pool includes species from the major hydrocarbon classes present in aviation fuels, namely *n*-alkanes, *iso*-alkanes, *cyclo*-alkanes, and aromatics, which exhibit distinct physicochemical characteristics due to differences in their chemical structures. By including species from multiple hydrocarbon classes, the candidate pool was designed to provide sufficient compositional flexibility for reproducing key physicochemical characteristics of the target fuel.

Table A1. Surrogate palette.

Class	Species	C	H
normal-alkanes	*n*-decane	10	22
	n-dodecane	12	26
	n-tridecane	13	28
	n-tetradecane	14	30
	n-hexadecane	16	34
iso-alkanes	*iso*-octane	8	18
	iso-dodecane	12	26
	iso-cetane	16	34
cyclo-alkanes	ethylcyclohexane	7	14
	methylcyclohexane	8	16
	decalin	10	18
aromatics	toluene	7	8
	n-propylbenzene	9	12
	1,3,5-trimethylbenzene	9	12
	1,2,4-trimethylbenzene	9	12
	tetralin	10	12
	n-butylbenzene	10	14
	1-methylnaphthalene	11	10

The genetic algorithm (GA) control parameters used for surrogate-fuel formulation, including the population size, number of generations, the numbers of best and random samples retained per generation, the transfer (crossover) and mutation probabilities are summarized in Table A2. These parameters were kept fixed for all optimization cases to ensure consistent search behavior and a fair comparison of fitness improvement toward the target-fuel properties.

Table A2. Genetic algorithm parameters.

Parameter	Value
Population	3000
Generation	600
Best sample	800
Random sample	400
Probability of transfer	0.5
Probability of mutation	0.1

The population denotes the total number of individuals per generation. During the recombination process of the first objective function, best samples and random samples are randomly paired to form 600 parent pairs, and each pair generates five offspring to maintain a constant population size. When generating offspring, the mole fractions of each parent are transferred to the offspring according to the probability of transfer, followed by a normalization procedure to ensure that the sum of mole fractions equals unity. After offspring generation, random mole fractions are assigned to a fraction of individuals determined by the probability of mutation to enhance the diversity of the child generation.

To examine the robustness of the optimization process, the GA optimization was executed multiple times with different random initial populations. The final surrogate fuel was selected based on the most frequently obtained combination of chemical species among the repeated runs, as summarized in Table A3.

Table A3. Selection frequency of surrogate fuel compositions from repeated GA runs.

Chemical Compositions	Value [%]
n-dodecane, *iso*-cetane, methylcyclohexane, *n*-butylbenzene	42
n-dodecane, *iso*-dodecane, ethylcyclohexane, *n*-butylbenzene	44
n-hexadecane, *iso*-dodecane, methylcyclohexane, *n*-butylbenzene	6
n-dodecane, *iso*-dodecane, ethylcyclohexane, 1,2,4-trimethylbenzene	4
n-tetradecane, *iso*-dodecane, methylcyclohexane, *n*-butylbenzene	4

The results show that a dominant combination of species consistently emerged across independent runs, indicating stable convergence of the optimization process. Across the 50 runs, feasible solutions consistently satisfied the imposed feasibility thresholds (density MAE = 20 kg/m^3 and ΔT_{pc} error = 5–15 K), indicating limited variability in the final outcomes. It was also observed that the optimization outcome is influenced by the empirically defined feasibility thresholds, which affect the selection of feasible candidates within the GA framework.

Appendix B

In the present study, the RK-PR equation of state was employed during the GA optimization due to its computational efficiency, while the NIST SUPERTRAPP database was used in the final comparison and heat transfer analysis. Accordingly, a comparative assessment between the two methods is provided in Figure A1.

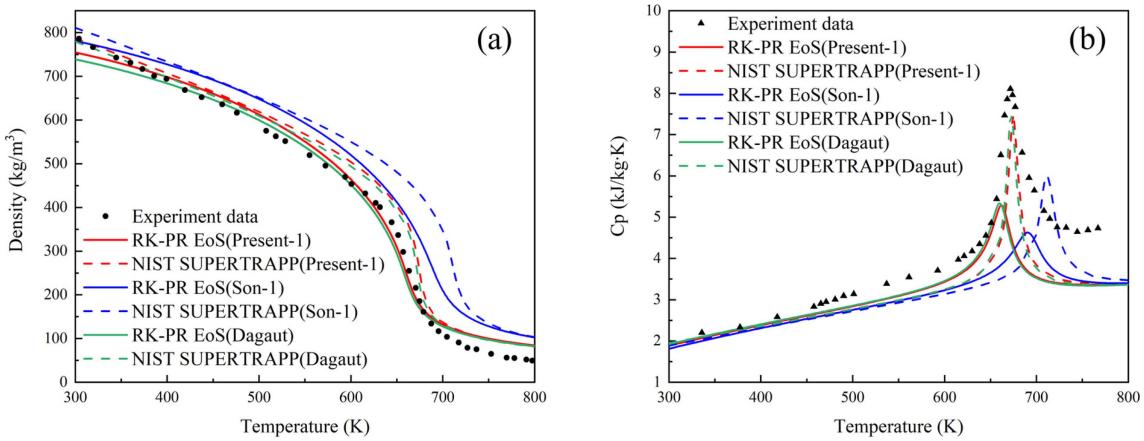


Figure A1. Comparison of thermophysical properties from RK–PR EoS, NIST SUPERTRAPP, and experimental data [28]: (**a**) density, (**b**) specific heat capacity at constant pressure.

Although some discrepancies exist in certain temperature ranges, the overall trends of density variation are in good agreement. In particular, the deviations are relatively small in the high-temperature region (above approximately 700 K), which is most relevant to supercritical heat transfer behavior. In addition, similar deviation trends are observed across all surrogate fuels, indicating consistent behavior of the RK-PR model.

For the specific heat (Cp), SUPERTRAPP predicts a more pronounced peak compared to RK-PR, resulting in a difference in the predicted pseudo-critical temperature (T_{pc}) between the two methods. This discrepancy is acknowledged. However, both methods consistently capture the location of rapid thermophysical property variation associated with the pseudo-critical region, which is the key factor governing heat transfer behavior.

Based on these observations, RK-PR is considered suitable for efficient surrogate fuel optimization, while SUPERTRAPP provides a more accurate reference for evaluating thermophysical properties and performing heat transfer analysis. Nevertheless, the observed discrepancies, particularly in Cp prediction and the resulting differences in T_{pc}, indicate a limitation of the present approach. Further refinement of the property prediction model or incorporation of higher fidelity thermophysical property data is required in future work to improve predictive accuracy.

Appendix C

To assess mesh independence, a series of structured grids (Mesh 1–Mesh 7) were generated using ICEM CFD. The operating conditions were fixed as follows: Present-1 was used as the working fluid, with a mass flow rate of 2.5 g/s, operating pressure of 3 MPa, and inlet temperature of 300 K. Heat transfer was applied to the lower outer wall of the test section. A convective heat transfer boundary condition was used, with the hot gas temperature and heat transfer coefficient set to 2400 K and 1100 W/m^2·K, respectively. The SST k–ω turbulence model was employed with the SIMPLEC pressure–velocity coupling scheme.

The structured grid was constructed using different strategies depending on the material properties and location. As illustrated in Figure A2, Block A denotes the corner region of the solid wall. In this region, a uniform mesh without inflation layers was applied. Block B represents the edges along the square channel, including both the fluid region and the adjacent solid region parallel to the channel. In these regions, inflation layers were applied with the first layer thickness set to 1×10^{-6} m to maintain y+ < 1, and the growth rate was set to 1.2 to properly resolve the thermal and velocity boundary layers.

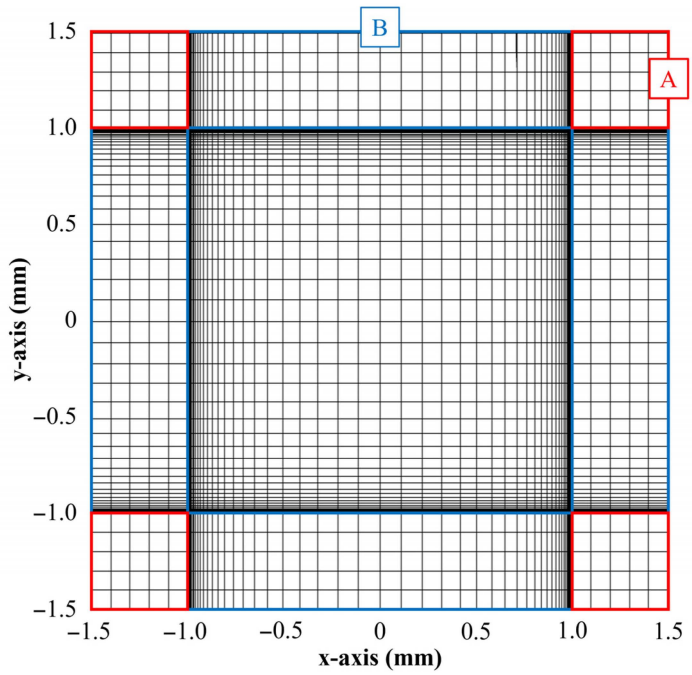


Figure A2. Mesh configuration used for the grid independence analysis.

As shown in Table A4, the numbers of edge divisions were systematically adjusted. Meshes 1–3 were constructed by progressively increasing the number of edge divisions in the fluid region. Meshes 4 and 5 were generated by increasing the mesh density in the solid region based on Mesh 2. Meshes 6 and 7 were constructed based on Mesh 2 by varying the cell size along the channel length within the test section.

Table A4. Edge division parameters and cell counts for each mesh.

Case	Edge Divisions (Block A)	Edge Divisions (Block B)	Test Section Edge Size (m)	Fluid Cells	Total Cells
Mesh 1	5	56	0.0005	6,262,592	8,969,022
Mesh 2	5	60	0.0005	7,189,200	10,071,918
Mesh 3	5	64	0.0005	8,179,712	11,238,750
Mesh 4	7	60	0.0005	7,189,200	11,238,750
Mesh 5	9	60	0.0005	7,189,200	12,469,518
Mesh 6	5	60	0.001	3,589,200	5,030,918
Mesh 7	5	60	0.00025	12,229,200	17,129,318

Heat transfer simulations were performed using the constructed meshes, and the wall temperature distribution was selected as the primary quantity of interest for the grid independence test. The corresponding wall temperature profiles for different mesh configurations are presented in Figure A3. The results showed that the coarsest cross-sectional mesh (Mesh 1) and the mesh with coarse axial resolution (Mesh 6) exhibited reduced prediction accuracy of the wall temperature in regions where localized heat transfer deterioration occurred. In contrast, the remaining meshes (Meshes 2–5 and 7) produced nearly identical wall temperature gradients. Consequently, considering both numerical accuracy and computational efficiency, Mesh 2 was selected for all subsequent simulations.

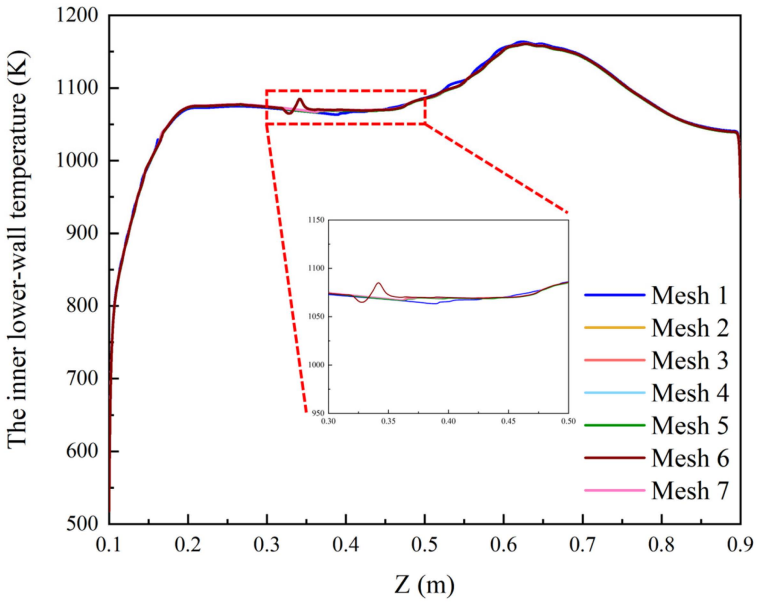


Figure A3. Wall temperature distributions for different mesh configurations.

References

1. Han, Z.; Zhou, W.; Zhao, X.; Jia, Z. Experimental study on convective heat transfer characteristics of supercritical pressure RP-3 kerosene in serpentine tubes. *Appl. Therm. Eng.* **2025**, *268*, 125954. [CrossRef]
2. Liu, J.; Xu, M.; Liu, P.; Xi, W. Heat transfer and flow structure characteristics of regenerative cooling in a rectangular channel using supercritical CO_2. *Aerospace* **2023**, *10*, 564. [CrossRef]
3. Xu, B.; Chen, B.; Peng, J.; Zhou, W.; Xu, X. A coupled heat transfer calculation strategy for composite cooling liquid rocket engine. *Aerospace* **2023**, *10*, 473. [CrossRef]
4. Jiang, J.; Wang, Y.; Xiao, Q.; Dong, R.; Li, J.; Wang, Z.; Fan, W. Experimental study on kerosene combustion under ambient, near-critical, and supercritical conditions for aero-engine applications based on CCA technology. *Aerospace* **2025**, *13*, 13. [CrossRef]
5. Zhou, W.; Xing, K.; Dou, S.; Yang, Q.; Xu, X. Experimental and numerical investigations on the mixing process of supercritical jet injected into a supersonic crossflow. *Aerospace* **2022**, *9*, 631. [CrossRef]
6. Zhang, J.; Zhou, Q.; Zhao, X.; Jiang, Y.; Fan, W. Numerical investigation on the heat transfer of n-decane in a horizontal channel with axially nonuniform heat flux under supercritical pressure. *Aerospace* **2022**, *9*, 326. [CrossRef]
7. Sun, F.; Li, Y.; Manca, O.; Xie, G. An evaluation on the laminar effect of buoyancy-driven supercritical hydrocarbon fuel flow and heat transfer characteristics. *Int. J. Heat Mass Transf.* **2019**, *142*, 118414. [CrossRef]
8. Chen, Y.; Li, Y.; Sunden, B.; Xie, G. The abnormal heat transfer behavior of supercritical n-decane flowing in a horizontal tube under regenerative cooling for scramjet engines. *Appl. Therm. Eng.* **2020**, *167*, 114637. [CrossRef]
9. Li, Y.; Markides, C.N.; Sunden, B.; Xie, G. Heat transfer deterioration in upward and downward pipe flows of supercritical n-decane for actively regenerative cooling. *Int. J. Therm. Sci.* **2021**, *168*, 107066. [CrossRef]
10. Li, Y.; Xie, G.; Sunden, B. Flow and thermal performance of supercritical n-decane in double-layer channels for regenerative cooling of a scramjet combustor. *Appl. Therm. Eng.* **2020**, *180*, 115695. [CrossRef]
11. Zhang, D.; Hou, L.; Gao, M.; Zhang, X. Experiment and modeling on thermal cracking of n-dodecane at supercritical pressure. *Energy Fuels* **2018**, *32*, 12426–12434. [CrossRef]
12. Hu, X.; Zhang, P.; Zhu, J.; Cheng, Z.; Sun, S. Numerical investigation of pyrolytic coking and its effects on heat transfer of RP-3. *Aerospace* **2025**, *12*, 919. [CrossRef]
13. Dooley, S.; Won, S.H.; Chaos, M.; Heyne, J.; Ju, Y.; Dryer, F.L.; Kumar, K.; Sung, C.-J.; Wang, H.; Oehlschlaeger, M.A.; et al. A jet fuel surrogate formulated by real fuel properties. *Combust. Flame* **2010**, *157*, 2333–2339. [CrossRef]
14. Won, S.H.; Haas, F.M.; Dooley, S.; Edwards, T.; Dryer, F.L. Reconstruction of chemical structure of real fuel by surrogate formulation based upon combustion property targets. *Combust. Flame* **2017**, *183*, 39–49. [CrossRef]
15. Bai, Y.; Wang, Y.; Wang, X.; Zhou, Q.; Duan, Q. Development of physical-chemical surrogate models and skeletal mechanism for the spray and combustion simulation of RP-3 kerosene fuels. *Energy* **2021**, *215*, 119090. [CrossRef]
16. Yu, Z.; Wei, S.; Wu, C.; Wu, L.; Sun, L.; Zhang, Z. Development and verification of RP-3 aviation kerosene surrogate fuel models using a genetic algorithm. *Fuel* **2022**, *312*, 122853. [CrossRef]
17. Yu, W.; Zhao, F. Formulating of model-based surrogates of jet fuel and diesel fuel by an intelligent methodology with uncertainties analysis. *Fuel* **2020**, *268*, 117393. [CrossRef]

18. Luo, S.; Xu, D.; Song, J.; Liu, J. A review of regenerative cooling technologies for scramjets. *Appl. Therm. Eng.* **2021**, *190*, 116754. [CrossRef]
19. Deng, H.W.; Zhu, K.; Xu, G.Q.; Tao, Z.; Zhang, C.B.; Liu, G.Z. Isobaric specific heat capacity measurement for kerosene RP-3 in the near-critical and supercritical regions. *J. Chem. Eng. Data* **2012**, *57*, 263–268. [CrossRef]
20. Deng, H.W.; Zhang, C.B.; Xu, G.Q.; Tao, Z.; Zhang, B.; Liu, G.Z. Density measurements of endothermic hydrocarbon fuel at sub- and supercritical conditions. *J. Chem. Eng. Data* **2011**, *56*, 2980–2986. [CrossRef]
21. Deng, H.W.; Zhang, C.B.; Xu, G.Q.; Zhang, B.; Tao, Z.; Zhu, K. Viscosity measurements of endothermic hydrocarbon fuel from (298 to 788) K under supercritical pressure conditions. *J. Chem. Eng. Data* **2012**, *57*, 358–365. [CrossRef]
22. Son, J.; Gil, Y.; Ko, S.; Shin, D.; Park, S. Development of jet surrogate fuel formulated by genetic algorithm. *Fuel* **2026**, *408*, 137590. [CrossRef]
23. Dagaut, P.; Cathonnet, M. The ignition, oxidation, and combustion of kerosene: A review of experimental and kinetic modeling. *Prog. Energy Combust. Sci.* **2006**, *32*, 48–92. [CrossRef]
24. Mao, Y.; Yu, L.; Qian, Y.; Wang, S.; Wu, Z.; Raza, M.; Zhu, L.; Hu, X.; Lu, X. Development and validation of a detailed kinetic model for RP-3 aviation fuel based on a surrogate formulated by emulating macroscopic properties and microscopic structure. *Combust. Flame* **2021**, *229*, 111401. [CrossRef]
25. Cheng, Z.; Tao, Z.; Zhu, J.; Wu, H. Diameter effect on the heat transfer of supercritical hydrocarbon fuel in horizontal tubes under turbulent conditions. *Appl. Therm. Eng.* **2018**, *134*, 39–53. [CrossRef]
26. Kim, S.; Choi, H.; Kim, Y. Thermodynamic modeling based on a generalized cubic equation of state for kerosene/LOx rocket combustion. *Combust. Flame* **2012**, *159*, 1351–1365. [CrossRef]
27. Cismondi, M.; Mollerup, J. Development and application of a three-parameter RK-PR equation of state. *Fluid Phase Equilib.* **2005**, *232*, 74–89. [CrossRef]
28. Wang, Y.; Hua, Y.; Meng, H. Numerical studies of supercritical turbulent convective heat transfer of cryogenic-propellant methane. *J. Thermophys. Heat Transf.* **2010**, *24*, 490–500. [CrossRef]
29. Huber, M.L. *NIST Thermophysical Properties of Hydrocarbon Mixtures Database (SUPERTRAPP)*, Version 3.2; NIST: Gaithersburg, MD, USA, 2007.
30. Kim, J.S.; Nam, H.; Kim, K.H. Development of supercritical heat transfer models for hydrocarbon fuels based on buoyancy: JP-8, JP-10, and n-dodecane. *Fuel* **2025**, *397*, 135233. [CrossRef]
31. Joh, M.; Kim, S.; Choi, H. Estimation of thermodynamic/transport properties of kerosene using a 3-species surrogate mixture. *J. Korean Soc. Aeronaut. Space Sci.* **2013**, *41*, 874–882. [CrossRef]
32. Gil, Y.; Ko, S.; Jang, S.P.; Park, S. Distinct roles of critical pressure and temperature in supercritical heat transfer of binary hydrocarbon mixtures for regenerative cooling. *Appl. Therm. Eng.* **2026**, *295*, 130652. [CrossRef]
33. Li, F.; Li, Z.; Jing, K.; Wang, L.; Zhang, X.; Liu, G. Thermal cracking of endothermic hydrocarbon fuel in regenerative cooling channels with different geometric structures. *Energy Fuels* **2018**, *32*, 6524–6534. [CrossRef]
34. Zhang, S.; Qin, J.; Xie, K.; Feng, Y.; Bao, W. Thermal behavior inside scramjet cooling channels at different channel aspect ratios. *J. Propuls. Power* **2016**, *32*, 57–70. [CrossRef]
35. Menter, F.R. Two-equation eddy-viscosity turbulence models for engineering applications. *AIAA J.* **1994**, *32*, 1598–1605. [CrossRef]
36. Deng, H.; Zhang, C.; Xu, G.; Tao, Z.; Zhu, K.; Wang, Y. Visualization experiments of a specific fuel flow through quartz-glass tubes under both sub- and supercritical conditions. *Chin. J. Aeronaut.* **2012**, *25*, 372–380. [CrossRef]
37. Li, Y.; Yang, K.; Wang, Z.; Pan, Y.; Wang, N.; Zhan, T. Convective heat transfer of hydrocarbon fuels in regenerative cooling channels with topologically optimized cross-sectional shapes. *Appl. Therm. Eng.* **2025**, *269*, 126151. [CrossRef]
38. Pu, H.; Chang, H.; Wang, J.; Shang, Y.; Dong, M.; Li, S. Experimental investigation and analysis of convective heat transfer to supercritical pressure aviation kerosene RP-3 in vertical miniature tubes based on the pseudo-boiling theory. *Appl. Therm. Eng.* **2023**, *219*, 119651. [CrossRef]
39. Ma, J.; Liu, H.; Xie, M. Exploring the relationship between heat transfer and pseudo-boiling for trans/supercritical real-fluid injection. *Int. J. Therm. Sci.* **2024**, *202*, 109063. [CrossRef]

Disclaimer/Publisher's Note: The statements, opinions and data contained in all publications are solely those of the individual author(s) and contributor(s) and not of MDPI and/or the editor(s). MDPI and/or the editor(s) disclaim responsibility for any injury to people or property resulting from any ideas, methods, instructions or products referred to in the content.